Combined methane reforming in presence of CO_2 and O_2 over $LaFe_{1-x}Co_xO_3$ mixed-oxide perovskites as catalysts precursors

M.R. Goldwasser [a,*], M.E. Rivas [a], M.L. Lugo [a], E. Pietri [a], J. Pérez-Zurita [a],
M.L. Cubeiro [a], A. Griboval-Constant [b], G. Leclercq [b]

[a] Centro de Catálisis, Petróleo y Petroquímica, Escuela de Química, FAC. Ciencias, UCV, Apartado 40600, Los Chaguaramos, Caracas, Venezuela
[b] Université des Sciences et Technologies de Lille, Laboratoire de Catalyse UMR 8010, Bât C3, 59655 Villeneuve D'Ascq, Cedex, France

Abstract

The paper deals with the effect of modification with cobalt of a series of $LaFe_{1-x}Co_xO_3$ mixed-oxide perovskites as catalyst precursors in the combined reforming of methane with CO_2 and O_2 for the production of syngas. The perovskite type oxides were synthesized by fine chemical using the citrate sol–gel method and characterized by techniques such as FT-IR, BET surface area, X-ray photoelectron spectroscopy (XPS), X-ray diffraction (XRD), TPR and inductively coupled plasma emission spectroscopy (ICP), under the condition of as-synthesized, reduced and used samples. The results showed that through this synthesis it is possible to obtain highly crystalline, homogeneous and pure solids, with well-defined structures. After reduction, the stabilization by the presence of iron of highly dispersed Co metallic particles from the cation on position B over the corresponding oxides was evidenced, decreasing deactivation by avoiding the sintering of metals and coke formation on the surface of the catalysts.

The existence of strong Fe–Co interaction in the $LaFe_{1-x}Co_xO_3$ with $x = 0.4$–0.6 produces a synergetic effect improving methane conversion and H_2 production.
© 2005 Elsevier B.V. All rights reserved.

Keywords: Combine methane reforming; Syngas production; $LaFe_{1-x}Co_xO_3$ mixed-oxide perovskites

1. Introduction

One of the most serious problems in CO_2 methane reforming is catalysts deactivation by coke. Since the reaction is endothermic, it proceeds at high temperature, thermodynamically favoring coke formation. Recently, CO_2 reforming of methane and steam *reforming* combined with partial oxidation has been studied [1–6]. Oxygen addition to these reactions reduces carbon deposition on the catalyst surface and increases methane conversion. Simultaneously, economical advantages are obtained by the appropriate combination of highly endothermic processes with the exothermic partial oxidation of methane by decreasing the energetic requirements of the reaction.

Similarly, the type of catalyst used could also inhibit coke formation [7–11]. The use of perovskite type oxides emerge as an alternative since after reduction it is possible to produce highly disperse metallic particles, diminishing deactivation of the catalyst by suppressing the coke forming reactions [1,7–9]. The catalytic activity of the mixed-oxide perovskites can be highly improved by partial substitution on A- and/or B-sites cations. B-cations could be partially reduced to well disperse metallic species supported on the A-site cation oxide, which make them ideal catalyst precursors for a series of reactions involving metals as active sites [1,2,7,8,12,13]. Similarly, the ease of removal or insertion of oxygen in perovskite type mixed-oxide materials provides an ideal framework for oxidation catalysis [1,2,10,13].

Addition of a second transition metal cation on B-site position such as cobalt to iron mixed-oxide perovskites should decrease the temperature at which these important

* Corresponding author. Fax: +58 212 239 21 62.
  E-mail address: mgoldwas@reacciun.ve (M.R. Goldwasser).

processes occur and increase specific conversion in methane partial oxidation [14–16].

The combine reaction then emerges as an interesting alternative since it improves the temperature control of the reactor and reduces formation of cold points. Besides, it allows the production of syngas with a broad range of H_2/CO ratios by manipulating the relative concentrations of O_2 and CO_2 in the feed.

In this paper, we present the results of the effect of modifying $LaFeO_3$ mixed-oxide perovskites with cobalt to produce a series $LaFe_{1-x}Co_xO_3$ ternary perovskites with $x = 0$ for $LaFeO_3$ and $x = 1$ for $LaCoO_3$ as catalyst precursors in the combine reforming of methane in the presence of CO_2 and O_2 for the production of syngas.

2. Experimental

The experimental procedure used for the synthesis and characterization of the mixed-oxide perovskites are similar to that previously reported in reference [7]. Description follows, adequate to the new synthesized solids.

2.1. Synthesis and characterization of the precursor perovskites

The studied mixed-oxide perovskites $LaFeO_3$, $LaFe_{0.8}Co_{0.2}O_3$, $LaFe_{0.6}Co_{0.4}O_3$, $LaFe_{0.4}Co_{0.6}O_3$, $LaFe_{0.2}Co_{0.8}O_3$ and $LaCoO_3$ were synthesized by fine chemical using a modification of the citrate sol–gel method [7,17]. Adequate amounts of the precursor of the cation at B-position were dissolved under vigorous stirring in a solution of citric acid (99.5 Riedel-de Haën) with an excess of ethylene glycol (99.5 Riedel-de Haën) as the organic polydentate ligand. The citric acid/B-cation molar ratio was 4, while it was 1.38 for ethylene glycol/citric acid. The mixture was kept at 50–60 °C with mild continuous stirring until a clear solution was obtained. At this point, a stoichiometric quantity of the precursor of cation A, $La(NO_3)_3 \cdot 5H_2O$, was added while keeping the mixture at 60 °C. The evaporating process proceeded for 2 days until a viscous resin was formed. The resin was dried at 150 °C for 24 h and calcined in air at 700 °C for 5 h.

The solids were characterized before and after catalytic tests by mass and surface physico-chemical techniques such as inductively coupled plasma emission spectroscopy (ICP) using a Perkin-Elmer ICP/5500 instrument to analyze the chemical compositions (Fe, Co and La) of the synthesized solids. Oxygen was determined by coulometric titration converting the oxygen to carbon oxides after passing over carbon at 1120 °C. The IR spectra of the final product were recorded in a Perkin-Elmer 283 spectrometer in the range 1200–400 cm^{-1}. The surface areas were measured by a single-point BET procedure using nitrogen–argon adsorption at −196 °C with an N_2/Ar ratio of 30/70 on a Micromeritics Model ASAP 2010. X-ray diffraction (XRD) experiments

were conducted using a Siemens D-8 advanced diffractometer with a Cu Kα radiation for crystalline phase detection between 20° and 90° (2θ) and under temperature program reduction in H_2 atmosphere (3 L/h) from room temperature to 800 °C. JCPDS-ICDD standard files software was used to determine the phases. The metallic crystallite sizes were calculated using metal (1 0 1) reflection and the Scherrer formula [18,19] with Warren's correction for instrumental line broadening $dv = 0.9\lambda/[(\beta^2 - B^2)^{1/2} \cos\theta]$, where $\lambda = 1.54056$ Å and the line broadening at 44°, 2θ, is $B = 0.09°$, by means of TOPAS P Profile Fitting Program from Brucker Analytical X-Ray System. The reducibility of these precursor mixed-oxide perovskites was studied by TPR and in situ XRD. The TPR was carried out in a Thermo-Quest TPD/TPR 1100 system using 0.07 g of the sample in 8 vol.% H_2/92 vol.% Ar stream (20 mL/min). The temperature was raised from room temperature to 120 °C at a rate of 10 °C/min, then holding it for 15 min to remove any adsorbed water, and raised again up to 900 °C for 2 h. The X-ray photoelectron spectroscopy (XPS) analyses were performed with a VG ESCALAB 220 XL spectrometer. The monochromatized Al Kα (1486.6 eV) source was operated at 80 W. The residual vacuum at the analysis chamber was always better than 5×10^{-8} Torr. For the XPS analyses, the reduction treatments were conducted in situ using H_2 as reducing agent and left 9 h at 500 °C (heating rate 2 °C/min). Auto-coherent references were used: La 3d (La^{3+}, 529 eV), Co 2p (Co^{3+}, 780.2 eV), Fe 2p (Fe^{3+}, 710 eV) and O 1s (529.3 eV). The binding energy of C 1s (284.6 eV) was used as an internal standard.

2.2. Activity test

The variation of the activity/selectivity patterns as a function of the composition of the mixed-oxide precursors, the influence of activation procedure and reaction parameters were monitored using 200 mg of catalyst in a 20-mm i.d. quartz reactor at atmospheric pressure operated in a fixed-bed continuous flow system with $CH_4/CO_2 = 1$ for the CO_2 reforming and $CH_4/CO_2/O_2 = 4/1/2$ for the combine reforming. Argon was used as diluent, 750–850 °C, and 24 L h^{-1} g^{-1} hourly space velocities. Before the catalytic tests, the solids were reduced in H_2 flow (20 mL/min, $T = 700$ °C, 8 h). After reduction, the system was swept with Ar for 15 min and adjusted to reaction temperature. The water produced during reaction, was condensed before passing the reactants and products to the analyzing system, which consisted of an on-line gas chromatograph (Perkin-Elmer Auto System XL) equipped with a TCD detector and provided with a Carbosieve SII 80/100 column (12′ × 1/8′ o.d. SS), as previously described [1]. The CH_4 and CO_2 conversions are defined as the CH_4 and CO_2 converted per total amount of CH_4 and CO_2 fed, respectively. The selectivity for product "i" was calculated based in carbon balance and defined as $S_i (\%) = N_i/(NCH_4(c) + NCO_2(c))100$, where $NCH_4(c)$ and $NCO_2(c)$ are the amounts of methane and carbon dioxide converted.

Table 1
Chemical composition of synthesized mixed-oxide perovskites

Perovskites	La (%)		Co (%)		Fe (%)		O (%)	
	n.	e.	n.	e.	n.	e.	n.	e.
$LaFeO_3$	57.22	55.12	–	–	23.00	22.26	19.77	20.55
$LaFe_{0.8}Co_{0.2}O_3$	57.07	54.78	4.84	5.03	18.35	17.49	19.72	18.56
$LaFe_{0.6}Co_{0.4}O_3$	56.93	54.54	9.66	9.83	13.73	13.09	19.67	17.70
$LaFe_{0.4}Co_{0.6}O_3$	56.78	53.05	14.45	14.27	9.13	8.49	19.62	19.81
$LaFe_{0.2}Co_{0.8}O_3$	56.64	45.78	19.22	15.90	4.55	5.76	19.57	19.07
$LaCoO_3$	56.50	52.49	23.97	23.79	–	–	19.52	18.23

n.: nominal values and e.: experimental values.

3. Results and discussion

3.1. Perovskite synthesis and ICP analysis

Table 1 shows the series of synthesized mixed-oxide perovskites and their chemical composition. The experimental values for each element are, within experimental error, very similar to the theoretical values, indicating a close coincidence between experimental and nominal molecular formula for the mixed-oxide perovskites assessing the benefits of the citrate sol–gel method to produce highly crystalline and homogeneous structures. However, it is important to point out that with the exception of $LaFe_{0.4}Co_{0.6}O_3$ and $LaFeO_3$ most mixed-oxide perovskites showed an oxygen deficiency in the structure.

3.2. IR, surface area and X-ray diffraction

IR and XRD analysis were performed to assess the formation of the perovskite structure. The IR spectra for all solids showed two broad bands characteristics of ABO_3 mixed-oxide centered at 400 and 600 cm^{-1}. Their positions are in good agreement with those reported in the literature [20]. Table 2 gives values of the observed position for the IR bands and the BET specific surface area measured after calcination. For the IR results, it can be observed that v_1 increases as Co substitutes Fe indicating that Co–O bond is stronger than that of Fe–O. As seen from Table 2, most of the synthesized solids showed areas higher than 3 m^2/g, the usual value obtained when mixed-oxide perovskites are prepared by other methods. In agreement with Bedel et al. observation [10], the specific surface areas of the perovskites

Table 2
BET specific surface area and IR bands position

Perovskite	Area (m^2/g)	IR band position	
		v_1 (cm^{-1})	v_2 (cm^{-1})
$LaFeO_3$	6	553	401
$LaFe_{0.8}Co_{0.2}O_3$	4	577	380
$LaFe_{0.6}Co_{0.4}O_3$	3	598	396
$LaFe_{0.4}Co_{0.6}O_3$	7	609	428
$LaFe_{0.2}Co_{0.8}O_3$	5	613	430
$LaCoO_3$	4	599	427

correspond mainly to the geometrical surfaces of the spherical particles, characteristic of nonporous grains. A clear relationship between the observed specific areas and the degree of substitution of iron by cobalt was not observed. However, a tendency to smaller surface areas in going from $LaFeO_3$ to $LaCoO_3$ was observed (Table 2).

For the binary perovskites, the room temperature XRD analyses reveal the presence of very crystalline orthorhombic $LaFeO_3$ (JCPDS-ICDD 15-0148) and rhombohedral $LaCoO_3$ (JCPDS-ICDD 48-0123) structures. All ternary mixed-oxide perovskites could also be indexed with orthorhombic or rhombohedral symmetry depending on the Fe–Co composition. The different types of structure obtained for all ternary mixed-oxide perovskites are listed in Table 3.

The XRD analyses of the as-synthesized solids at room temperature revealed the perovskite structure as the main phase for all synthesized solids with high crystalline and well-defined symmetry. It was observed that for the high Co containing perovskites the more intense peaks are doublets, characteristic of the $LaCoO_3$ structure with formation of

Table 3
In situ XRD results: symmetry, phases and average size of Co (Fe) after reduction

Solid	Symmetry[a]	2θ[b] (°)	T of degradation (°C)	Main phases after reduction	Particle size (nm)
$LaFeO_3$	O	32.221	800	Fe^0, La_2O_3, $LaFeO_3$,	51.9
$LaCo_{0.2}Fe_{0.8}O_3$	O	32.696	800	La_2O_3, Co^0, Fe^0, Fe_2O_3	41.3
$LaCo_{0.4}Fe_{0.6}O_3$	O	32.928	700–800	La_2O_3, Co^0, Fe^0,	54.3
$LaCo_{0.6}Fe_{0.4}O_3$	R	32.954	600–700	La_2O_3, Co^0, Fe^0,	42.2
$LaCo_{0.8}Fe_{0.2}O_3$	R	33.125	600–700	La_2O_3, Co^0, Fe^0	28.3
$LaCoO_3$	R	33.174	300–400	La_2O_3, Co^0,	13.6

JCPDS-ICDD: Co^0 (01-1254), Fe^0 (01-1252), Co^0–Fe^0 (65-6829), La_2O_3 (05-0602), $LaFeO_3$ (JCPDS-ICDD 15-0148) and $LaCoO_3$ (JCPDS-ICDD 48-0123).
[a] R: rhombohedral and O: orthorhombic.
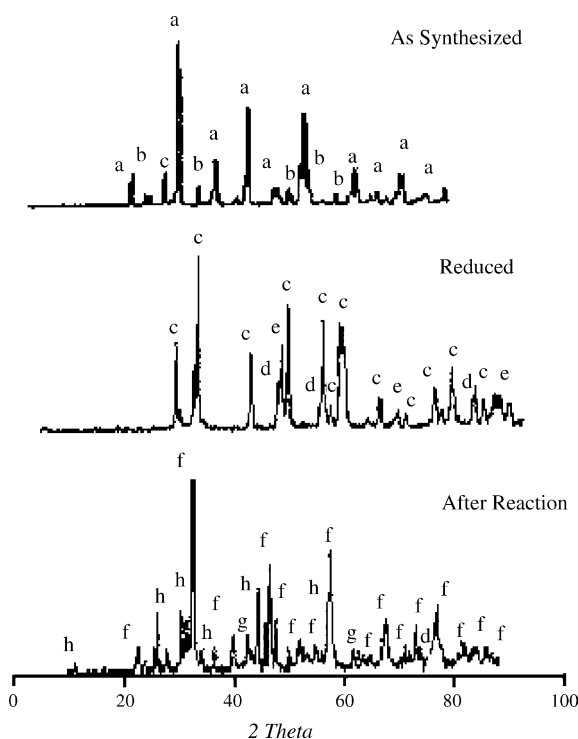[b] Evolution of the most intense peak at 29 °C.

Fig. 1. XRD pattern of $LaFe_{0.4}Co_{0.6}O_3$. Mixed-oxide perovskite (a) $LaCo_{0.6}Fe_{0.4}O_3$, (b) Fe_2O_3, (c) La_2O_3, (d) Co^0, (e) Fe^0, (f) $LaFeO_3$, (g) CoO and (h) $La_2O_2CO_3$.

Fig. 2. TPR profile of $LaFe_xCo_{1-x}O_3$ mixed-oxide perovskite type series.

La–Co spinel type intermediates, indicating the existence of a more complex structure.

As an example, the X-ray diffraction pattern of $LaCo_{0.6}Fe_{0.4}O_3$ as-synthesized, reduced and after reaction is shown in Fig. 1. After reduction, structural breakdown of the perovskite occur producing Co^0, Fe^0 and La_2O_3. However, the mayor phases detected after reaction were $La_2O_2CO_3$ and $LaFeO_3$ perovskite. This $LaFeO_3$ perovskite phase was observed for all studied series after reaction, which is not surprising due to the oxidative character of the reactants in the reforming reaction (CO_2 and O_2) and to the facility of iron to oxidize ($\varepsilon_{Fe^0} = -0.33\,V$).

3.3. TPR and in situ XRD studies

The reduction of the perovskite type oxides was also followed by TPR and in situ XRD analysis for all solids. For the binary mixed-oxide perovskites, it is observed that $LaFeO_3$ perovskite start reducing at 800 °C and it is not completely reduced even after 900 °C (Fig. 2). $LaCoO_3$ perovskite shows a first hydrogen consumption peak at around 380 °C, attributed to reduction of Co^{3+} species to Co^{2+}. The second hydrogen consumption peak is observed at around 580 °C, assigned to reduction of Co^{2+} species to Co^0, in agreement with a stepwise reduction.

A similar reduction behavior is also shown by the ternary mixed-oxide perovskites. A first peak observed at low temperature between 300 and 500 °C, while the second peak
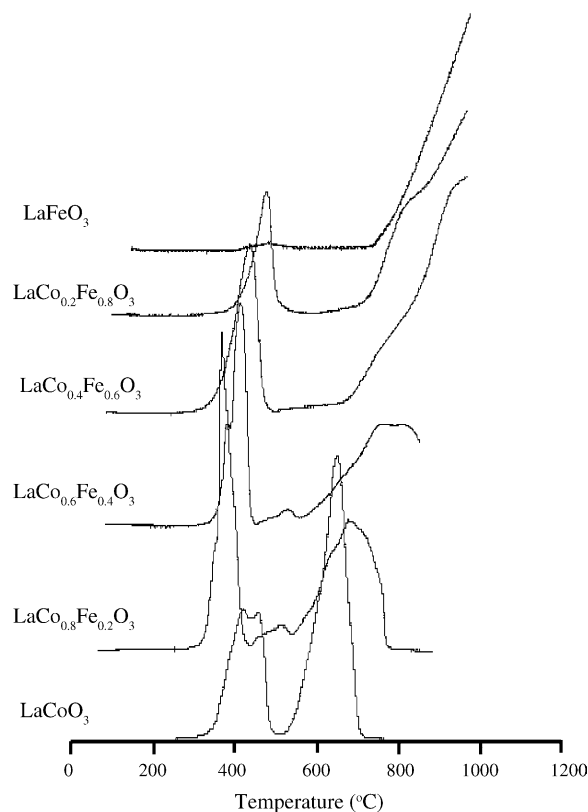
appears at around 560 °C. The temperature at which the second peak is observed varies with the iron content in the structure: as the amount of iron increases the reduction temperature also increases.

The reduction profiles for Fe–Co with $x \geq 0.4$ and the progressive shift to higher temperatures as x increases is mainly due to the partial reduction of Fe^{3+} to Fe^0, induced by the presence of Co^0 particles. An activated Fe reduction assisted by Co^0 particles seems to exist, which favors Fe–Co solid solutions formation after reduction. However, it is important to point out that this Fe–Co phase formation was detected mainly after reduction but no necessarily after reaction, where formation of an iron perovskite $LaFeO_3$ was observed, depending on the oxidation character of the reaction mixture (CO_2 or O_2).

These results were corroborated by in situ X-ray diffraction analyses. The binary perovskite $LaCoO_3$ showed a change between 300 and 400 °C, since the most intense signal corresponding to the perovskite structure shifted to lower 2θ values. For the ternary oxides with $x = 0.2$ and 0.4, the degradation temperature increases notably with the most intense peak shifting only after 600 °C, while those solids with $x = 0.6$ and 0.8 degradation starts at 700 °C. Finally, the $LaFeO_3$ binary perovskite, starts to reduce only after 2 h at 800 °C, indicating that an increase in the reduction facility of iron perovskite is attained when Fe is replaced by Co. As an example, the in situ X-ray diffraction of $LaCo_{0.6}Fe_{0.4}O_3$ is shown in Fig. 3.

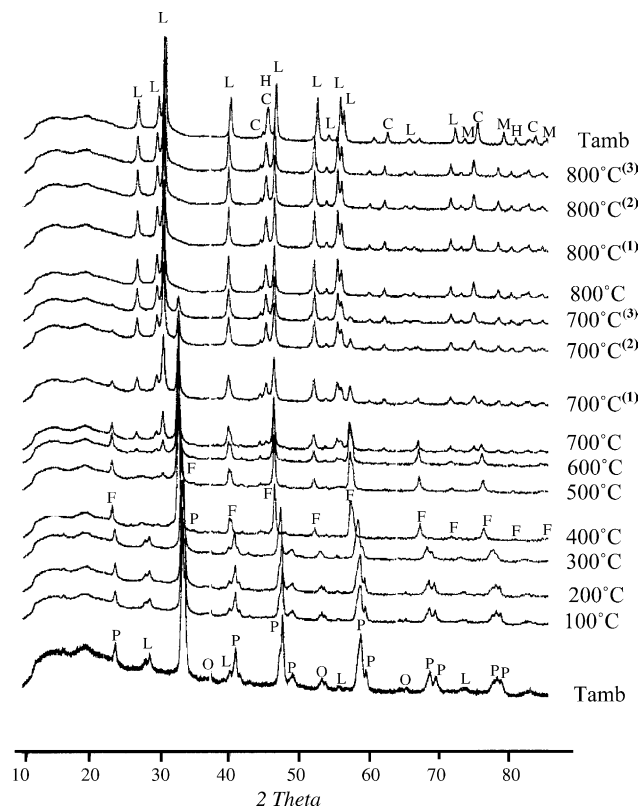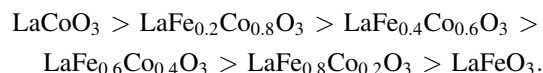Fig. 3. In situ X-ray diffraction of $LaCo_{0.6}Fe_{0.4}O_3$ mixed-oxide perovskite P: perovskite $LaCo_{0.6}Fe_{0.4}O_3$, L: La_2O_3, O: Co_3O_4, F: $LaFeO_3$, H: Fe^0, C: Co^0 and M: $CoO·Co_2O_3$; (#) time in hours at a given temperature.

For all solids, the observed phases after reduction at 800 °C were: Co^0 and Fe^0 dispersed on a La_2O_3, Fe_2O_3, CoO or Co_2O_3 matrix depending on the starting perovskite composition. Higher iron amount containing perovskites were more difficult to reduce.

The ease of reduction for this series was:

$$LaCoO_3 > LaFe_{0.2}Co_{0.8}O_3 > LaFe_{0.4}Co_{0.6}O_3 >$$
$$LaFe_{0.6}Co_{0.4}O_3 > LaFe_{0.8}Co_{0.2}O_3 > LaFeO_3.$$

XRD analysis was also used to determine the metal particles size of the crystallites by means of the Scherrer formula [18,19] using peaks at around 44–45°, 2θ, which corresponds to the most intense peak for Co^0 (44.216) and Fe^0 (44.354). The decomposition temperature, main phases present after reduction and particle size for all studied solids are presented in Table 3.

For all mixed-oxide perovskites, a decrease in particle size is observed as Co is incorporated to the structure. Perovskites with higher iron content and orthorhombic symmetry show bigger iron particle sizes as compared to cobalt rich perovskites. This result is not surprising since it is expected that higher iron content should lead to a decrease in dispersion. Similarly, iron rich perovskites degrade at higher temperatures (Table 3) which could lead to metal sintering. The lower particle size shown by $LaCo_{0.2}Fe_{0.8}O_3$ is attributed to the fact that under the used reduction conditions the iron species are not completely reduced, so the particle size determination was carried out on a mixture of metallic and oxides particles. As previously mentioned, for the less iron containing mixed-oxide perovskites the formation of a Fe–Co solid solution seems possible since the metallic particles of both metals appear at the same 2θ angle. Formation of a dioxomonocarbonate phase, $La_2O_2CO_3$, was also observed. It has been established that catalysts modified by lanthanum ions are characterized by the presence of the $La_2O_2CO_3$ phase on the surface increasing the thermal stability of the catalysts. This layer is in fast equilibrium with the carbon dioxide in the gas phase during reaction, and has also been claimed as responsible for inhibiting formation of deactivating coke [7,21–24].
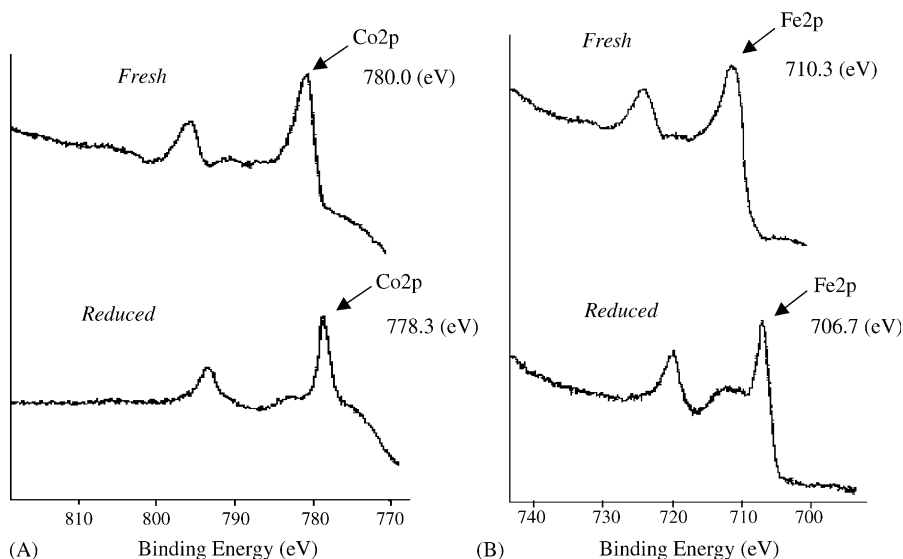

Fig. 4. XPS spectra of (A) Co 2p and (B) Fe 2p for $LaCo_{0.4}Fe_{0.6}O_3$ mixed-oxide perovskite fresh and reduced.

3.4. X-ray photoelectron spectroscopy analyses

X-ray photoelectron spectroscopy analyses was carried out for $LaFeO_3$, $LaFe_{0.6}Co_{0.4}O_3$ and $LaCoO_3$ mixed-oxide perovskites as-synthesized and after reduction to characterize the reducibility of B-site cations of the perovskite, surface species and chemical state of oxygen [25–29]. Depending on the studied perovskite, the presence of doublets characteristic of: La 4d (La^{3+}, 104.5 eV), Co 2p (Co^{3+}, 780.2 eV) and Fe 2p (Fe^{3+}, 710 eV) were observed on the fresh samples, together with two bands corresponding to O 1s at 529 and 531.5 eV.

After the reduction treatment the $LaCoO_3$ binary perovskite was completely destroyed. The XPS spectra showed a variation of the La 4d signal and the Co 2p doublet is placed at around 778.6 eV. This value corresponds to that reported for Co^0 (778.6 eV). Again, some bands attributed to the presence of carbonates were observed. No carbon rests bands were present.

The binary $LaFeO_3$ perovskite shows two components for Fe 2p, one at 711 eV attributed to the species Fe^{3+} and the other at 707 eV, corresponding to the presence of Fe^0 species, indicating that the perovskite structure is not completely reduced. Only one O 1s signal was observed after reduction and no evidence of carbon rests were detected.

Figs. 4 and 5 show the XPS spectra for the ternary $LaFe_{0.6}Co_{0.4}O_3$ mixed-oxide perovskite as-synthesized and reduced. The observed Co 2p doublet is placed at 778.6 eV (Fig. 4A), indicating again that the perovskite structure was destroyed; traces of oxides were also observed. The value obtained for the Fe 2p doublet at around 706 eV (Fig. 4B) indicate that after reduction iron on this solid is present mainly as Fe^0 (706.5 eV).

Table 4
Bulk and surface stoichiometry of the reduced perovskites

Perovskite	La	Co	Fe	O	Co/La	Fe/La	La/O
$LaFeO_3$							
Surface	1.00	–	0.26	1.15	–	0.26	0.87
Bulk	0.96	–	0.96	3.11	–	1.0	0.31
$LaCo_{0.4}Fe_{0.6}O_3$							
Surface	1.00	0.07	0.13	1.05	0.07	0.13	0.95
Bulk	0.96	0.40	0.57	2.69	0.4	0.59	0.37
$LaCoO_3$							
Surface	1.00	0.23	–	1.23	0.23	–	0.81
Bulk	0.92	0.99	–	2.80	1.1	–	0.33

Fig. 5 shows the La 4d and O 1s spectra for $LaFe_{0.6}Co_{0.4}O_3$. The La 4d signal of the fresh sample shows two less well-resolved peaks than those observed after reduction, corroborating the change of La from the perovskite structure to that of La_2O_3 and confirming the presence of La in two different environments (Fig. 5A).

For the O 1s signal, on the fresh perovskite, two bands are observed which suggest the contribution of oxygen in different chemical environments on the perovskite surfaces [25]. The band at 529 eV is attributed to oxygen's of the oxides structure (O^{2-} species) while that place at 531.5 eV is assign to less electron-rich species such as carbonates or other oxides [9] (Fig. 5B); after reduction, the peak at higher binding energy disappears. The C 1s band observed at 289 eV corroborates the presence of carbonates rests.

Table 4 shows the bulk and surface stoichiometry obtained for all solids. It is observed that only the cations in position B of the mixed-oxide perovskites (Co and Fe) are reduced to their zero oxidation state. Similarly, an enrichment of La in the surface is observed. The (O)/(La)
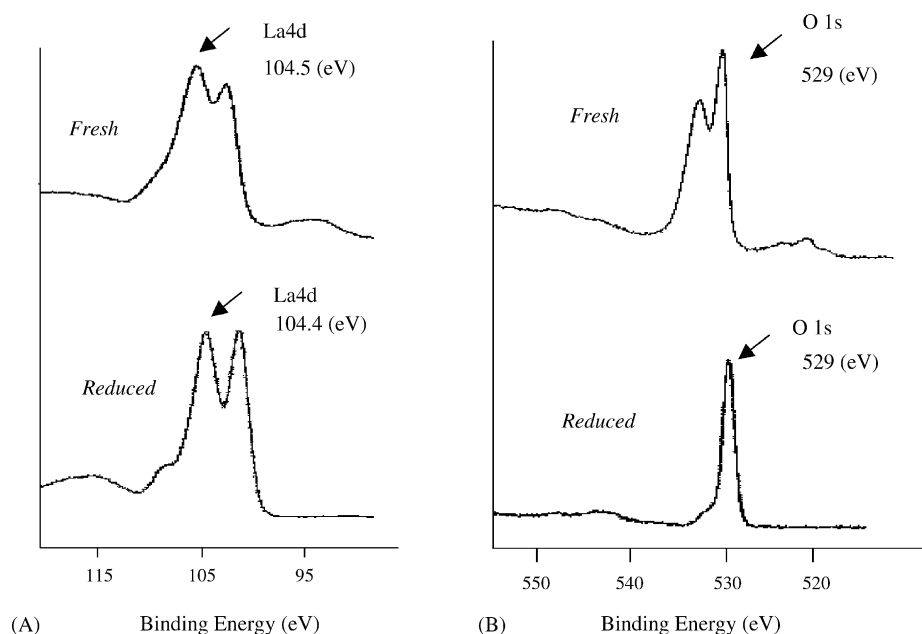

Fig. 5. XPS spectra of (A) O 1s and (B) La 4d for $LaCo_{0.4}Fe_{0.6}O_3$ mixed-oxide perovskite fresh and reduced.

Table 5
Combined reforming of methane in the presence of CO_2 and O_2

Perovskite	XCH_4 (%)	XCO_2 (%)	$H_2/CH_{4(Conv)}$	$H_2/CO_{(molar)}$
$LaFeO_3$	34	7	0.25	1.78
$LaCo_{0.2}Fe_{0.8}O_3$	51	−2	1.13	0.88
$LaCo_{0.4}Fe_{0.6}O_3$	80	76	3.21	1.81
$LaCo_{0.6}Fe_{0.4}O_3$	81	77	1.37	1.96
$LaCo_{0.8}Fe_{0.2}O_3$	65	43	3.15	1.75
$LaCoO_3$	84	48	1.34	0.82

$t_r = 24$ h, WHSV = 24 L/(h g), $CH_4/CO_2 = 1$, $CH_4/O_2 = 2$, $W = 200$ mg, $T_r = 800\ ^\circ C$ and $T_{red} = 700\ ^\circ C$ (8 h).

ratio indicates an oxygen deficiency for these solids being more marked for the $LaFeO_3$ binary perovskite, in agreement with TPR and XRD analyses.
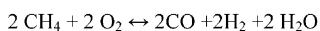
3.5. Activity results

The results of the catalytic test for the combined reforming of methane with CO_2 and O_2 are shown in Table 5. In the experimental conditions used the catalytic conversion could be due to partial oxidation of methane, CO_2 reforming or combination of combustion and steam reforming. Several possibilities have to be considered to analyze the observed results:
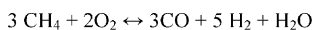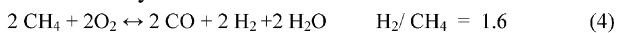
First possibility

$$CH_4 + 1/2\ O_2 \leftrightarrow CO + 2H_2 \qquad H_2/CH_4 = 2 \quad \chi CH_4 = \chi CO_2 \quad (1)$$

$$\underline{CH_4 + CO_2 \leftrightarrow 2CO + 2H_2 \qquad\qquad H_2/CO = 1.3 \qquad\qquad\qquad (2)}$$

$$2\ CH_4 + CO_2 + 1/2\ O_2 \leftrightarrow 3CO + 4\ H_2$$

Second possibility

$$CH_4 + 2O_2 \leftrightarrow CO_2 + 2H_2O \qquad H_2/CH_4 = 1 \qquad\qquad\qquad\qquad (3)$$

$$\underline{CH_4 + CO_2 \leftrightarrow 2CO + 2H_2 \qquad\qquad H_2/CO = 1 \qquad\quad \chi CO_2 \sim 0}$$

$$2\ CH_4 + 2\ O_2 \leftrightarrow 2CO + 2H_2 + 2\ H_2O$$

Simultaneously

$$2\ CH_4 + 2O_2 \leftrightarrow 2\ CO + 2\ H_2 + 2H_2O \qquad H_2/CH_4 = 1.6 \qquad (4)$$

$$\underline{CH_4 + H_2O \leftrightarrow CO + 3\ H_2 \qquad\qquad\qquad H_2/CO = 1.6 \qquad\qquad (5)}$$

$$3\ CH_4 + 2O_2 \leftrightarrow 3CO + 5\ H_2 + H_2O$$

$$CO_2 + H_2 \leftrightarrow CO + H_2O \text{ (RWGS)} \qquad\qquad\qquad\qquad\qquad\qquad (6)$$
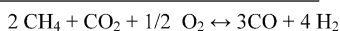
For the studied solids, the higher activity is shown by those with a higher Co content: $LaCoO_3$, $LaCo_{0.6}Fe_{0.4}O_3$ and $LaCo_{0.4}Fe_{0.6}O_3$. For $LaCo_{0.6}Fe_{0.4}O_3$, the H_2/CO ratio was close to 2, which indicates that reactions (1) and (2) are the main occurring reactions. This catalyst showed also a higher surface area than the rest of the solids. However, the observed deviation of the experimental values of the ($H_2/CH_{4(Conv)}$) ratio respect to the theoretical indicate that a series of possible reactions such as reactions (3), (5) and (6) are taken place. The $H_2/CH_{4(Conv)}$ ratios equal or higher than 3 indicate that syngas is produced by the steam reforming reaction (reaction (5)) from the water obtained by

methane combustion (reaction (3)). Over $LaFeO_3$, a typical oxidation catalyst, the $H_2/CH_{4(Conv)}$ ratio smaller than 1 indicate that the reverse water gas shift reaction (reaction (6)) is taken place, which consume hydrogen and is favored at high temperature.

For the higher iron containing mixed-oxide perovskites, $LaFeO_3$ and $LaCo_{0.2}Fe_{0.8}O_3$, methane conversion was always higher than that of CO_2, which indicates that on those catalysts methane combustion is favored (reaction (3)).

The results shown in Table 5 indicate that the partial substitution of iron by cobalt in the B-site position of the perovskite, highly improved their catalytic activity producing a marked promoter effect on the catalysts. Zhong et al. [30] using $LaFe_{1-y}A_yO_3$ mixed-oxide perovskites showed that the specific activity of the catalysts in the oxidation of methane is higher than that of $LaFeO_3$, and the extension of the effect depends on the nature of A-cation. Similarly, Provendier et al. [14] on Fe–Ni perovskite show the stabilization of Ni by Fe. These authors propose that Fe controlled the reversible migration of Ni during reaction forming alloys which hinder the Ni sintering.

4. Conclusions

All synthesized solids showed homogeneous and highly crystalline perovskite type structure as evidenced by X-ray diffraction and IR analyses.

TPR results show that substitution of Fe by Co favors iron reduction probably due to an activated Fe reduction induced by Co. XRD results suggest the presence of a strong Fe–Co interaction for the $x = 0.4$–0.6 ratio, in agreement with Bedel et al. observations [10].

XPS results revealed the existence of different oxygen species with different chemical environments on the perovskite surfaces.

The simultaneous oxidative and CO_2 reforming reaction of methane notably diminish coke formation, increasing syngas production. The addition of oxygen to the $CH_4 + CO_2$ system decreases the reaction temperature and the energy consumption, indicating that the partial oxidation (exothermic) reaction promotes the dry (endothermic) reaction, in agreement with Tomishige et al. results for Ni/Al_2O_3 and Pt/Al_2O_3 catalysts [31] and for NiO–MgO solid solution catalyst [32].

The partial substitution of iron by cobalt in the B-site position of the perovskite produces a significant promoter effect enhancing the catalytic activity of the solids. After reduction, highly dispersed Co particles stabilized by iron over the corresponding oxide are observed, decreasing metal sintering and coke formation on the catalyst surface.

The catalytic results show that the combine reaction proceeds initially by methane combustion followed by CO_2 and H_2O reforming. The heat liberated by the methane combustion favors the reforming reaction. Substitution of Fe

by Co inhibits methane combustion increasing both CO_2 conversion and the $H_2/CH_{4(Conv)}$ ratio.

A synergic effect seems to exist for the 0.4–0.6 Fe/Co molar ratio since $LaFe_{0.6}Co_{0.4}O_3$ and $LaFe_{0.4}Co_{0.6}O_3$ under optimize experimental conditions show high activity and selectivity with a $H_2/CO \sim 2$ molar ratio, probably due to a higher oxygen concentration on the perovskite surface as evidence from ICP and XPS analyses.

Acknowledgement

References

[1] M.R. Goldwasser, M.E. Rivas, E. Pietri, M.J. Pérez-Zurita, M.L. Cubeiro, A. Grivobal-Constant, G. Leclercq, J. Mol. Catal. A: Gen. 228 (2005) 325.

[2] T. Utaka, S. Al-Drees, J. Ueda, Y. Iwasa, T. Takeguchi, R. Kikuchi, K. Eguchi, Appl. Catal. A: Gen. 247 (2003) 125–131.

[3] M.A. Pena, J.P. Gomez, J.L.G. Fierro, Appl. Catal. A: Gen. 144 (1996) 7.

[4] Y. Lu, J. Xue, C. Yu, Y. Liu, S. Shen, Appl. Catal. A 174 (1998) 121.

[5] A.M. O'Connor, J.R.H. Ross, Catal. Today 46 (1998) 203.

[6] K. Otsuka, Y. Wang, E. Sunada, I. Yamanaka, J. Catal. 175 (1998) 152.

[7] M.R. Goldwasser, M.E. Rivas, E. Pietri, M.J. Pérez-Zurita, M.L. Cubeiro, L. Gingembre, L. Leclercq, G. Leclercq, Appl. Catal. A: Gen. 255 (2003) 45.

[8] E. Pietri, A. Barrios, O. Gonzalez, M.R. Goldwasser, M.J. Pérez-Zurita, M.L. Cubeiro, J. Goldwasser, L. Leclercq, G. Leclercq, Stud. Surf. Sci. Catal. 136 (2001) 381.

[9] J.L.G. Fierro, Catal. Today 8 (1990) 153.

[10] L. Bedel, A.C. Roger, C. Estournes, A. Kiennemann, Catal. Today 85 (2–4) (2003) 207.

[11] J.B. Wang, S.-Z. Hsiao, T.-J. Huang, Appl. Catal. A: Gen. 246 (2003) 197.

[12] T. Hayakawa, S. Suzuki, J. Nakamura, T. Uchijima, S. Hamakawa, K. Suzuki, T. Shihido, K. Takehira, Appl. Catal. A: Gen. 183 (1999) 273.

[13] A.R. Chakhmouradian, R.M. Mitchell, P.C. Burns, J. Alloys Compd. 307 (2000) 149.

[14] H. Provendier, C. Petit, C. Estournes, S. Libs, A. Kiennemann, Appl. Catal. A 180 (1999) 163.

[15] K. Takehira, T. Shishido, M. Kondo, J. Catal. 207 (2002) 307.

[16] W. Chu, W. Yang, L. Lin, Appl. Catal. A 235 (2002) 39.

[17] M.P. Pechini, United States Patent Office, 3,330,673 (1967).

[18] M.C.J. Bradford, M.A. Vannice, Appl. Catal. A: Gen. 142 (1996) 73.

[19] H.P. Klug, L.E. Alexander, X-Ray Diffraction Procedures for Polycrystalline and Amorphous Materials, Wiley, London, 1962 , p. 491.

[20] C.P. Khattak, D.E. Cox, Mater. Res. Bull. 12 (1977) 463.

[21] N. Matsui, K. Anzai, N. Akamatsu, K. Nakagawa, N. Okikenaga, T. Suzuki, Appl. Catal. A: Gen. 179 (1999) 247.

[22] V.A. Tsipouriari, X.E. Verykios, Catal. Today 64 (2001) 83.

[23] T. Le Van, M. Che, M. Kermarec, C. Louis, J.M. Tatibouët, Catal. Lett. 6 (1990) 395.

[24] A. Olafsen, A.-K. Laesson, H. Fjellvag, B.C. Hauback, J. Solid State Chem. 158 (2001) 14.

[25] Q. Xu, D. Huang, W. Chen, H. Wang, B. Wang, R. Yuan, Appl. Surf. Sci. 228 (2004) 110.

[26] D. Waller, J.A. Lane, J.A. Kilner, B.C.H. Steele, Mater. Lett. 27 (1996) 225.

[27] A.R. Chakhmouradian, R.M. Mitchell, P.C. Burns, J. Alloys Compd. 307 (2000) 149.

[28] D. Waller, J.A. Lane, J.A. Kilner, B.C.H. Steele, Solid State Ionics 86–88 (1996) 767.

[29] G.C. Kostogloudis, C. Ftikos, Solid State Ionics 126 (1999) 143.

[30] Z. Zhong, K. Chen, Y. Ji, Y.Q. Yan, Appl. Catal. A: Gen. 156 (1997) 29.

[31] K. Tomishige, S. Kanazawa, K. Suzuki, M. Asadullah, M. Sato, K. Ikushima, K. Kunimori, Appl. Catal. A: Gen. 233 (2002) 35.

[32] K. Tomishige, Catal. Today 89 (2004) 405.